# Automatic detection of abrupt patient motion in SPECT data acquisition

Elisabeth Röhl, Hanno Schumacher, Bernd Fischer

Institute of Mathematics, University of Lübeck, Wallstrasse 40, 23560 Lübeck, Germany

## ABSTRACT

Due to the long imaging times in SPECT, patient motion is inevitable and constitutes a serious problem for any reconstruction algorithm. The measured inconsistent projection data leads to reconstruction artefacts which can significantly affect the diagnostic accuracy of SPECT, if not corrected. Among the most promising attempts for addressing this cause of artefacts, is the so-called data-driven motion correction methodology. To use this approach it is necessary to automatically detect patient motion and to subdivide the acquired data in projection sets accordingly. In this note, we propose three different schemes for automatically detecting patient motion. All methods were tested on 3D academic examples with different rigid motions, motion times, and camera systems. On the whole, every method was tested with approximately 400 to 600 test cases. One of the proposed new methods does show promising results.

**Keywords:** Image restoration and enhancement

## 1. INTRODUCTION

In Single Photon Emission Computed Tomography (SPECT), the imaging time is typically in the range of 5-30 minutes. Here, patient movement, which has frequently been reported in clinical applications,[1] constitutes a serious problem for any reconstruction scheme. The movements cause misalignment of the projection frames, which degrades the reconstructed image and may introduce artefacts. These motion artefacts may significantly affect the diagnostic accuracy.[2–4] Different methods have been proposed for the correction of motion in SPECT studies. These methods may be divided into three categories. The first two approaches do produce motion corrected projections and thus may be used in conjunction with any reconstruction method. The first approach is purely hardware based, like, for example the triple scan[5] or dual scan[6] protocol. The second approach corrects for the patient motion by using a computational method applied within the projection-space.[7,8] It should be noted, that due to the projection geometry the latter method is not able to compensate for rotational movement. In this paper, we are concerned with the third methodology. Here the correction is performed in the image space. A widely used member out of this class is the so-called data driven motion correction (DDMC) approach.[9,10] It can handle full rigid-body motion. To start the scheme, it is assumed that the point in time of the rigid-body motion of the patient during the SPECT imaging is known. Once the point in time of the motion is known this motion needs to be corrected. The idea is to subdivide the projection data into $l$ subsets or motion-sets where no motion has been detected and to estimate the motion in between these subsets accordingly by using a partial reconstruction of the subset containing the largest number of projections and calculate a suitable transformation in order to fit it to the other subsets. To this end the rigid-body parameters after the $k$th movement of the patient are stored in the vector $T_k$. Furthermore, all projections that were measured between the $k$th and the $k+1$st movement are collected in the projection set $\mathcal{P}_k$. The image, which has been in the course of the algorithm reconstructed up to the $k$th step, is denoted by $\mathbf{f}^{(k)}$. This image has to be corrected with respect to the next object position $T_{k+1}$. The result is denoted by $\mathbf{f}^{(k)}(T_{k+1})$. Next the partial reconstruction $\mathbf{f}^{(k)}(T_{k+1})$ is updated with the help of measured projections $\mathcal{P}_{k+1}$ via

$$\mathbf{f}^{(k+1)} = \mathbf{R}[\mathcal{P}_{k+1}, \mathbf{f}^{(k)}(T_{k+1})], \tag{1}$$

Further author information: (Send correspondence to Elisabeth Röhl)
Elisabeth Röhl: E-mail: roehl@informatik.uni-luebeck.de
Hanno Schumacher: E-mail: schumaha@math.uni-luebeck.de
Bernd Fischer: E-mail: fischer@math.uni-luebeck.de

where $\mathbf{R}$ denotes a reconstruction algorithm. Ideally, the resulting image $\mathbf{f}^{(l)}$ should contain less motion artefacts. But this approach has two main disadvantages. The first is the motion estimation using partial reconstructions. Due to this the quality of the motion estimation depends on the quality of the partial reconstruction, which is only of good quality if $\frac{1}{3}$ of all projections are in one subset. A scheme overcoming this disadvantage by combining reconstruction and motion correction can be found in.[11] The second is the needed information about the point in time of the patient motion during the SPECT imaging in order to subdivide the acquired projection into subsets with the same position of the patient. Up to now this is done by hand, or alternatively expensive external detection systems are used.[12,13] To avoid both of this modus operandi a fully automatic method, working only with the acquired projection data, is wanted. However such a method is only useful if it detects reliably any occurring motion for every given configuration of camera heads in a SPECT. In this note we investigate three different methods and perform a sound testing for the proposed Methods. These three methods are introduced in Section 2 and tested for 3D academic images in Section 3. Finally, some conclusions are drawn in Section 4.

## 2. METHODS

Given SPECT projection data $\mathbf{P}$ containing $m$ angularly equidistant projections of a 3D object, we aim for subdividing these data into subsets of projections with the same object position $\mathcal{P}_1, \ldots, \mathcal{P}_l$ with $l$ as the number of different object positions. The intention is to perform this task fully automatically only using the measured projection data. The following three methods were investigated and tested against this requirement.

### 2.1. Using the Mean Square Difference

The first method, the mean square difference (MSD), was introduced by Hutton et al.[10,14] as a part of the DDMC approach. But so far it has not been tested how accurate it detects occurring motion automatically. Furthermore the MSD was only designed for SPECT systems with perpendicular camera heads.

Within this method a first step is to reconstruct the measured projection data $\mathbf{P}$. Afterwards this reconstruction is forward-projected and will be denoted as $\mathbf{P^{fp}}$. Subsequently the measured projections and the forward-projections are compared using the MSD. This is done by calculating the MSD between the $k$-th 2D projection $\mathbf{P}_k$ and $\mathbf{P^{fp}}_k$ for all $k = 1, \ldots, m$ by

$$\mathrm{MSD}(k) = \mathrm{MSD}(\mathbf{P}_k, \mathbf{P^{fp}}_k) = \frac{\sum_{i=1}^{n_1} \sum_{j=1}^{n_2} (\mathbf{P}_k(i,j) - \mathbf{P^{fp}}_k(i,j))^2}{n_1 n_2} \tag{2}$$

where $n_1$ and $n_2$ are the number of rows and columns of the projections. If a dual or triple head SPECT is used, the simultaneously acquired projections have the same object position. To incorporate this fact the MSD values for these simultaneously acquired projections is added together. Ideally, projections with the same object position have the same MSD value. An idealized result for a dual head SPECT imaging using 60 projections, perturbed with two motions, is shown in fig. 1. Therefore occurring motion in the acquired data can be detected by searching a changeover between $\mathrm{MSD}(\mathbf{P}_k, \mathbf{P^{fp}}_k)$ and $\mathrm{MSD}(\mathbf{P}_{k+1}, \mathbf{P^{fp}}_{k+1})$. Which is done using the difference quotient

$$\mathrm{DQ}_k = \mathrm{MSD}(\mathbf{P}_k + 1, \mathbf{P^{fp}}_k + 1) - \mathrm{MSD}(\mathbf{P}_k, \mathbf{P^{fp}}_k) \tag{3}$$

with $k = 1, \ldots m$ and $DQ_m = \mathrm{MSD}(m) - \mathrm{MSD}(1)$. Additionally a threshold $\theta_{data}$ is needed in order to differentiate if a changeover occurs because of motion or due to variations caused by discretization, rounding errors, or noise. To find $\theta_{data}$ automatically, we simply used the average and the standard deviation

$$\theta_{data} = \overline{\mathrm{DQ}} + \sqrt{\frac{1}{m-1} \sum_{i=1}^{m} (DQ_i - \overline{\mathrm{DQ}})^2} \tag{4}$$

of the difference quotients DQ. In order to prevent a large amount of false-positively detected motion when no motion occurred or the used method is blind towards that kind of motion, we introduced a default value $\theta_{def}$. Now the used threshold $\theta$ is calculated using

$$\theta = (\text{number of cameras}) \max\{\theta_{def}, \theta_{data}\}. \tag{5}$$

Experience has shown that for the MSD method $\theta_{def} = \overline{\mathrm{DQ}} + 5$ is a good value.

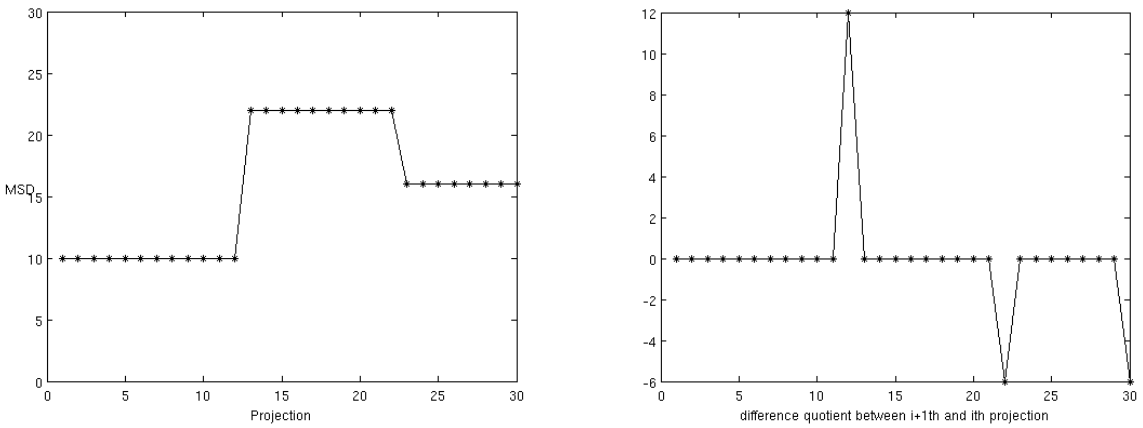


Figure 1: An idealized result of the MSD with two motions for a dual head SPECT imaging using 60 projections (left). After using the difference quotient one can see after which projection motion occurs (right).

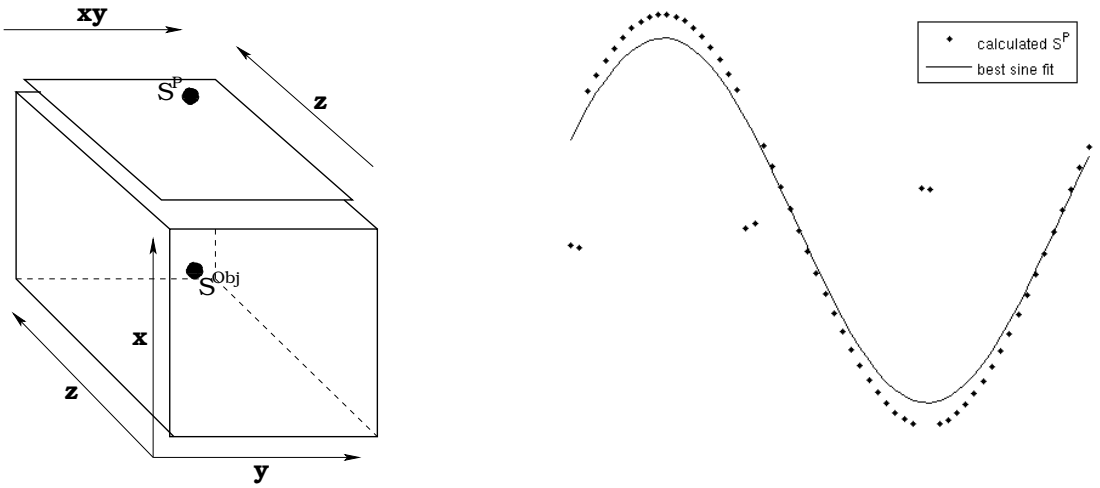


Figure 2: On the left side the CoM of an object and the CoM of a projection. For some conditions the CoM of the projection is the projected CoM of the object. Additionally the used coordinate system can be seen with the z-axis as the rotation axis of a SPECT system. On the right side the resulting curve of the CoM xy-coordinate for all measured projections (dotted) of a motion perturbed SPECT imaging and a best sine fit through these coordinates (solid).

### 2.2. Using the Center of Mass

The second method to detect motion is based on the center of mass (CoM) of the measured projections $\mathbf{P}$. Under the assumption of absorption free projection the projected CoM of an object is identical with the CoM of any projection $\mathbf{P}_k$, $k = 1, \ldots, m$ acquired from this object and can be calculated by

$$S^{\mathbf{P}_k} = \frac{\sum_{i=1}^{n_1} \sum_{j=1}^{n_2} \mathbf{P}_k(i,j) \begin{pmatrix} i \\ j \end{pmatrix}}{\sum_{i=1}^{n_1} \sum_{j=1}^{n_2} \mathbf{P}_k(i,j)} \tag{6}$$

where $n_1$ and $n_2$ are the number of rows and columns of the projections. So the CoM can be used as a landmark in the object whose position is known in every projection. We suggest two different ways of analyzing these data to detect motion in the SPECT imaging.

The first method uses the projection geometry of a SPECT system. Due to this plotting all xy-coordinates of the CoM of a motion free SPECT imaging should result in a sin-curve and is constant for all z-coordinates. The used coordinate system is defined in fig. 2 with the z-axis of the object as the rotation axis of a SPECT system. Now the idea is to interpret all $S^{\mathbf{P}_k}$ coordinate wise and perform a best sine fit through the xy-coordinates of the CoM (see fig 2). This can be done because it is known from the SPECT camera gantry that the coordinates in the first direction form a sine and are constant in the other direction, if the measured data is motion free. If motion occurs these forms should be perturbed as shown for the xy-coordinate in (fig.2). So the sine curve is subtracted from the xy-coordinates of all CoMs and, like in the MSD approach, the difference quotient is applied to the resulting curve and to all z-coordinates to detect possible motion. Like in the MSD scheme the knowledge that simultaneously acquired projections belongs to the same object position is used. This is done by adding the values coming up from the difference quotient of these projections. Finally, to analyze these two curves the average, the standard deviation, and a threshold are calculated and every value not fitting in this range is defined as motion.

In the second method the measured data are reconstructed first to calculate a forward-projection. Afterwards the coordinates of the CoM are calculated in every projection $\mathbf{P}_k$ and $\mathbf{P^{fp}}_k$. Next for every $k = 1, \ldots, m$ $S^{\mathbf{P}_k}$ and $S^{\mathbf{P^{fp}}_k}$ are subtracted and interpreted coordinate-wise as a curve. Again, to detect motion the difference quotient, the average, the standard deviation, and a threshold are used to detect a changeover in the run of these curves. Experience has shown that for both center of mass methods $\theta_{def} = \overline{\mathrm{DQ}} + 0.01$ is a good value. Like in the first CoM method the data of simultaneously acquired projections are added after the difference quotient.

### 2.3. Using CoM and Principal Axis

The third and last method uses a combination of the CoM and principal axes. First the measured data $\mathbf{P}$ is reconstructed to calculate a forward-projection generates $\mathbf{P^{fp}}$ thereafter. Now the projections $\mathbf{P}_k$ and $\mathbf{P^{fp}}_k$, $k = 1, \ldots, m$ are considered as density functions or mass distributions. So the *expectation value* $\mathbb{E}$ of a function $f : \mathbb{R}^n \to \mathbb{R}$ with respect to projection $\mathbf{P}_k$ is defined as

$$\mathbb{E}^{\mathbf{P}_k}(f(x,y)) = \frac{\sum_{i=1}^{n} \sum_{j=1}^{m} f(x_i, y_j) \mathbf{P}_k(i,j)}{\sum_{i=1}^{n} \sum_{j=1}^{m} \mathbf{P}_k(i,j)}, \tag{7}$$

which can also be interpreted as the CoM of the projection $\mathbf{P}_k$. Furthermore the *covariance* is generated by

$$Cov^{\mathbf{P}_k} := \mathbb{E}^{\mathbf{P}_k}[(x - S^{\mathbf{P}_k})(x - S^{\mathbf{P}_k})^T] \in \mathbb{R}^{2\times 2}. \tag{8}$$

The principal axes is now given as a line through the CoM in the direction of an eigenvector corresponding to the largest eigenvalue of the covariance.[15] Now the coordinates of the center of mass are analyzed as in the second version of the CoM methods. Additionally the angle between the principal axes of $\mathbf{P}_k$ and $\mathbf{P^{fp}}_k$ can be calculated to gain a third criterion for motion detection. The idea is that in a motion free imaging the principal axes of $\mathbf{P}_k$ and $\mathbf{P^{fp}}_k$ are equal and the angle between both axes will be zero. But if motion occurs an angle greater than zero should be detected. So the angle between all projections $\mathbf{P}_k$ and $\mathbf{P^{fp}}_k$ are calculated and analyzed with the difference quotient, the average, the standard deviation, and a threshold. Experience has shown that for the principal axis $\theta_{def} = \overline{\mathrm{DQ}} + 1.15^\circ$ is a good value. Also in this case the information coming up from simultaneously acquired data are used together.

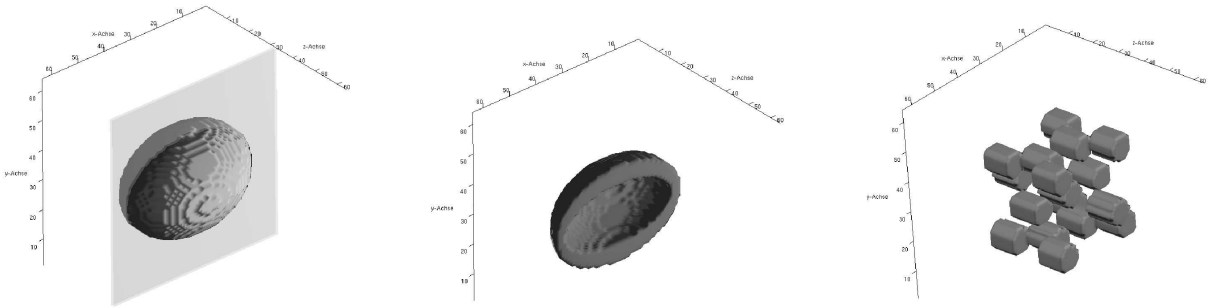

(a) First phantom

(b) First phantom cut on the layer shown in 3a

(c) Second phantom

Figure 3: Used phantoms.

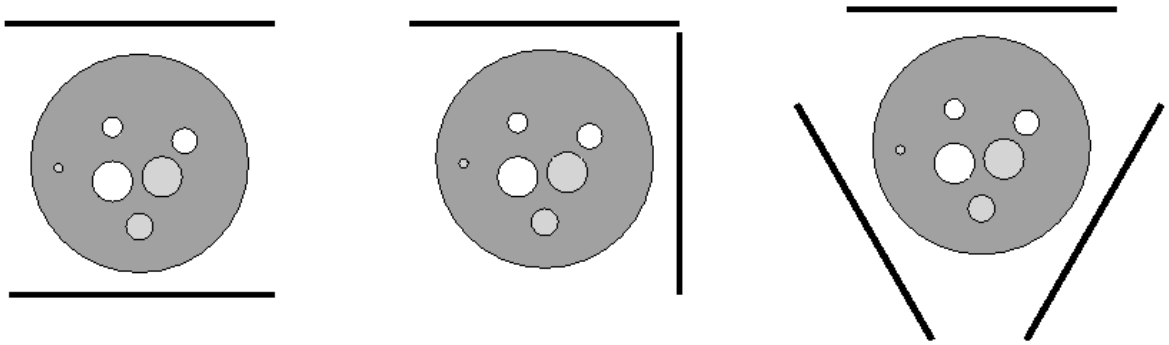

Figure 4: Three types of SPECT systems are tested. From left to right: opposing heads (1), perpendicular heads (2) and three heads with an angle of 120 degree between the cameras (3).

## 3. RESULTS

To test the introduced methods, two 3D discrete academic phantoms with a resolution of $64 \times 64 \times 64$ voxels were created. The first one looks like a coconut, the second one consists of seventeen small separated cylinders (see fig.3). Three different types of SPECT systems are tested (see fig. 4). The first two systems are dual head SPECT, one with opposite heads, the other with perpendicular heads. The last system is a triple head SPECT with an angle of 120 degree between the cameras. For these three systems a SPECT imaging is simulated using the two introduced phantoms. For the dual head system with opposing heads and the triple head system a 360 degree imaging using 60 projections is simulated and a 180 degree imaging with 30 projections for the perpendicular heads. As a first step the phantoms are noise-free and absorption or scattering is not included in the simulated imaging.

To reconstruct the calculated projections we choose the well known expectation maximization (EM) algorithm[16] using 20 iterations. To test the methods for motion detection two scenarios are used. In the first scenario one motion occurs during the SPECT imaging. To test all methods systematically translation of $0.5, 1.0, 2.5, 5.0$ pixels tested separate in x- y- and z-direction. The same is done for rotation of $2, 3.5, 9$ and 18 degrees around all three axis. Additionally 15 motion sets using all six degrees of freedom were randomly created using a range of $-5$ to 5 pixel for translation and $-18$ to 18 degrees for rotation. These ranges were chosen to guarantee a motion greater than 0.5 pixel, due to the fact that motion of half a pixel or more can end up in motion artefacts after reconstruction.[17] In the second scenario two motions occurred during the SPECT imaging. In this case only the randomly created 15 motion sets are used. For both motion scenarios table 1 defines after which projection motion occurs. The projection number was chosen randomly. For the camera systems using 60 projections four different sets for the point in time when motion occurs are defined and three sets for the system using 30 projections.

| Camera system | 1 | 2 | 3 |
|---|---|---|---|
| Number of projections | 60 | 30 | 60 |
| Rotation angle | 360° | 180° | 360° |
| One motion after projection | 14 | 3 | 14 |
| | 7 | 8 | 7 |
| | 9 | 14 | 9 |
| | 27 | | 3 |
| Two motions after projection | 14, 15 | 3, 7 | 14, 15 |
| | 7, 17 | 8, 11 | 7, 17 |
| | 9, 13 | 14, 15 | 9, 13 |
| | 27, 29 | | 3, 19 |

Table 1: Tested motion scenarios for all three camera systems (see fig. 4).

| | $CoM_1$ | $CoM_2$ | CoM + PA | MSD |
|---|---|---|---|---|
| detected motion in percent | 93.84 | 93.66 | 95.83 | 69.20 |
| false-positive rate of all det. motions in percent | 31.30 | 26.87 | 63.24 | 72.52 |

Table 2: Results for the dual head SPECT system with opposing heads. Altogether 552 motions must be detected to reach 100%. From left to right: first center of mass version, second center of mass version, center of mass with principle axes, and mean squared difference.

The results for all motion tests to any defined motion position for the three different camera systems are shown in table 2, 3, and 4. The tables present the detection rate and the false-positive detection rate in percent. The false-positive rate is calculated using the number all detected positions without motion divided by the number of all detection. Table 2 specifies the results for the dual head SPECT with opposing heads, table 3 for perpendicular heads, and table 4 for the triple head SPECT system.

Both CoM versions detect approx. 93% of all motions with a low rate of false-positive detected motions for SPECT system (2) and (3) (see fig. 4) and approx. 30% for system (1). Comparing both versions one should prefer the second one. It always has a little higher detection rate and a lower false-positive detection rate. But it has the disadvantage that a reconstruction and forward-projection of the acquired data are needed, which need much more computing time as the sine-fit of the first version. Unfortunately using the CoM has a general drawback. It obviously cannot detect rotation if the center of rotation is identical with the CoM. In this case the CoM will not change. Due to this one more criterion should be used to detect motion like in the CoM with principle axes method. For all three camera systems, using this combined center of mass and principle axes approach, approx. 96% of the occurring motion could be detected. But more than 50% of the detected motions are false-positive detections. As one can see from the false-positive rate of the CoM methods most of the false-positive detected motions are coming up from the angle informations of the principal axes. On the other hand this method can detect motion which is not seen in MSD or CoM. Further tests combining these method with the DDMC approach are needed to decide if it is problematic to detect $2n$ motions if only $n$ motions occur. The last method, the MSD, can only detect 70% up to 80% of all occurring motion. Additionally it has a false-positive detection rate depending on the used camera system of 72%, 35%, and 9%. One should note that this method was only build for SPECT systems with perpendicular heads. But even for that system the

| | $CoM_1$ | $CoM_2$ | CoM + PA | MSD |
|---|---|---|---|---|
| detected motion in percent | 91.79 | 92.75 | 96.86 | 69.32 |
| false-positive rate of all det. motions in percent | 7.99 | 3.76 | 50.80 | 35.07 |

Table 3: Results for the dual head SPECT system with perpendicular heads. Altogether 414 motions must be detected to reach 100%. From left to right: first center of mass version, second center of mass version, center of mass with principle axes, and mean squared difference.

| | $CoM_1$ | $CoM_2$ | CoM + PA | MSD |
|---|---|---|---|---|
| detected motion in percent | 92.57 | 92.75 | 96.20 | 79.89 |
| false-positive rate of a det. motion in percent | 0.00 | 0.00 | 66.33 | 9.07 |

Table 4: Results for the triple head SPECT system. Altogether 552 motions must be detected to reach 100%. From left to right: first center of mass version, second center of mass version, center of mass with principle axes, and mean squared difference.

MSD detection rate is much lower comparing to the other methods. Due to this, one of the three other methods should be used.

## 4. DISCUSSION

We presented and evaluated three methods for automatically detecting rigid body motion in SPECT imaging working with the acquired projection data only. One of these methods, using a center of mass approach combined with information on principle axes, does exactly detect the motion in most cases (96%). Unfortunately, it works with a high false-positive detection rate (60 %). The method using the CoM only, has a lower false-positive rate for the price that it detects less motion occurrences. Future work will investigate the high false-positive rate of the principle axes approach in more detail. Furthermore, to advance the detection rate of the center of mass approach it is planned to employ one more criterion for motion detection and to evaluate this method for real SPECT data. Finally, the best motion detection approach will be included in the DDMC scheme for further testing.

## REFERENCES


1. J. Wheat and G. Currie, "Incidence and characterization of patient motion in myocardial perfusion spect: Part 1," *Journal of Nuclear Medicine Technology* **32**, pp. 60–65, June 2004.
2. E. H. Botvinick, Y. Y. Zhu, W. J. O'Connell, and M. W. Dae, "A quantitative assessment of patient motion and its effect on myocardial perfusion SPECT images," *J Nucl Med* **34**(2), pp. 303–310, 1993.
3. J. A. Cooper, P. H. Neumann, and B. K. McCandless, "Effect of patient motion on tomographic myocardial perfusion imaging," *J Nucl Med* **33**(8), pp. 1566–1571, 1992.
4. J. Friedman, K. Van Train, J. Maddahi, A. Rozanski, F. Prigent, J. Bietendorf, A. Waxman, and D. S. Berman, ""upward creep" of the heart: A frequent source of false-positive reversible defects during thallium-201 stress-redistribution SPECT," *J Nucl Med* **30**(10), pp. 1718–1722, 1989.
5. C. Pellot-Barakat, M. Ivanovic, D. A. Weber, A. Herment, and D. K. Shelton, "Motion detection in triple scan SPECT imaging," *IEEE Trans Nucl Sci* **45**(4), pp. 2238–2244, 1998.
6. A. M. Passalaqua and R. Narayanaswamy, "Patient motion correction of SPECT images: dual scan approach," *IEEE Proc. NSSS'94, Norfolk, VA* **3**, pp. 1270–1274, 1995.
7. K. J. Lee and D. C. Barber, "Use of forward projection to correct patient motion during SPECT imaging," *Phys Med Biol* **43**, pp. 171–187, 1998.
8. Q.-s. Chen, P. R. Franken, M. Defrise, M. H. Jonckheer, and F. Deconinck, "Detection and correction of patient motion in SPECT imaging," *J Nucl Med Technol* **21**(4), pp. 198–205, 1993.
9. R. R. Fulton, S. Eberl, S. R. Meikle, B. F. Hutton, and M. Braun, "A practical 3D tomographic method for correcting patient head motion in clinical SPECT," *IEEE Trans Nucl Sci* **46**(3), pp. 667–672, 1999.
10. A. Z. Kyme, B. F. Hutton, R. Hatton, D. Skerrett, and L. Barnden, "Practical aspects of a data-driven motion correction approach for brain spect," *IEEE Transaction on Nuclear Science* **22**, pp. 722–729, June 2003.
11. H. Schumacher and B. Fischer, "A new approach for motion correction in spect imaging," in *In Bildverarbeitung für die Medizin. Springer. Accepted for publication.*, 2007.
12. R. Beach, H. P. Pretorius, G. Boening, P. P. Bruyant, B. Feng, R. R. Fulton, M. A. Gennert, S. Nadella, and M. A. King, "Feasibility of stereo-infrared tracking to monitor patient motion during cardiac spect imaging," *IEEE Trans. Nucl. Sci.* **51**(5), pp. 2693–2698, 2004.

13. P. Bruyant, M. Gennert, G. Speckert, R. Beach, J. Morgenstem, N. Kumar, S. Nadella, and M. King, "A robust visual tracking system for patient motion detection in spect: hardware solutions," in *IEEE Nuclear Science Symposium Conference Record*, **5**, pp. 3094– 3097, 2004.
14. B. F. Hutton, A. Z. Kyme, Y. H. Lau, D. W. Skerrett, and R. Fulton, "A hybrid 3-d reconstruction/registration algorithm for correction of head motion in emission tomography," *IEEE Transaction on Nuclear Science* **49**, pp. 188–194, February 2002.
15. J. Modersitzki, *Numerical Methods for Image Registration*, Oxford University Press, 2004.
16. F. Natterer and F. Wübbeling, *Mathematical Methods in Image Reconstruction*, Society for Industrial and Applied Mathematics, Philadelphia, 2001.
17. R. Eisner, A. Churchwell, T. Noever, and et al., "Quantitative analysis of the tomographic thallium-201 myocardial bullseye display: Critical role of correcting for patient motion," *Journal of Nuclear Medicine Technology* **29**, pp. 91–97, January 1988.